Underwater double vortex generation using 3D printed acoustic lens and field multiplexing

Chadi Ellouzi; Ali Zabihi; Farhood Aghdasi; Aidan Kayes ⓘ ; Milton Rivera; Jiaxin Zhong ⓘ ; Amir Miri ⓘ ;
Chen Shen ✉ ⓘ

Check for updates

View Online   Export Citation

03 April 2024 13:59:17

AIP Publishing

Underwater double vortex generation using 3D printed acoustic lens and field multiplexing

View Online   Export Citation   CrossMark

Chadi Ellouzi,[1] Ali Zabihi,[1] Farhood Aghdasi,[1] Aidan Kayes,[1] [ID] Milton Rivera,[1] Jiaxin Zhong,[2] [ID] Amir Miri,[3] [ID] and Chen Shen[1,a] [ID]

AFFILIATIONS

[1] Department of Mechanical Engineering, Rowan University, Glassboro, New Jersey 08028, USA

[2] Graduate Program in Acoustics, The Pennsylvania State University, Pennsylvania 16802, USA

[3] Department of Biomedical Engineering, New Jersey Institute of Technology, Newark, New Jersey 07102, USA

Note: This paper is part of the Special Topic on New Frontiers in Acoustic and Elastic Metamaterials and Metasurfaces.
[a] Author to whom correspondence should be addressed: shenc@rowan.edu

ABSTRACT

The generation of acoustic vortex beams has attracted an increasing amount of research attention in recent years, offering a range of functions, including acoustic communication, particle manipulation, and biomedical ultrasound. However, incorporating more vortices and broadening the capacity of these beams and associated devices in three dimensions pose challenges. Traditional methods often necessitate complex transducer arrays and are constrained by conditions such as system complexity and the medium in which they operate. In this paper, a 3D printed acoustic lens capable of generating a double vortex pattern with an optional focusing profile in water was demonstrated. The performance of the proposed lens was evaluated through computational simulations using finite element analysis and experimental tests based on underwater measurements. The results indicate that by altering the positioning of the vortices' axes, it is possible to control both the intensity and the location of the pressurized zone. The proposed approach shows promise for enhancing the effectiveness and versatility of various applications by generating a larger number of vortices and freely tailoring the focal profile with a single lens, thereby expanding the practical uses of acoustic vortex technology.

I. INTRODUCTION

In recent years, a lot of research effort has been devoted to acoustic vortices, driven by their potential applications in various fields, including the manipulation of particles, transmission of acoustic information, and imaging that surpasses the limitations imposed by wave diffraction.[1–5] Acoustic vortices share similar characteristics with their optical counterparts, notably featuring a unique helical pattern in their wavefront. At the center of the vortex lies an area of zero pressure and a distinctive phase singularity. In contrast to plane acoustic waves, acoustic vortex beams exhibit a distinct phase spiral that varies with the azimuthal angle. This twisting property is quantified by the topological charge, which indicates the number of complete rotations the beam's phase makes around the center axis in the span of one wavelength.[6–8] The topological charge plays a crucial role in determining the number of twists

and the direction of the acoustic vortex's phase spiral. Another notable aspect of acoustic vortices is their inherent orbital angular momentum, which holds the potential to be transferred to different materials or objects through wave–matter interactions. The ability to create acoustic vortices across a broad spectrum of frequencies allows for the handling of objects ranging from nanometers to centimeters. Along this line, acoustic vortices have been harnessed for the capture and rotation of objects in different media.[9–12] Li *et al.* employed a focused acoustic vortex, which was produced using a passive polydimethylsiloxane (PDMS) lens coupled with a single piezoelectric transducer set to operate at a frequency of 500 kHz, in order to trap particles.[13] In a separate study, a custom-made acoustic tweezer that functioned at a frequency of 43.5 MHz to create a vortex capable of seizing and accurately positioning individual cells from a group within a conventional microscopy setup was proposed by Baudoin *et al.*.[14] Furthermore, other studies

proposed a tornado-inspired acoustic vortex tweezer that produces a net acoustic force that is capable of non-intrusive intravascular trapping of lipid-encapsulated gas microbubbles within blood vessels. To achieve this, the proposed study employs a single 3 MHz concave transducer made of lead zirconate titanate (PZT).[15]

Another important application of acoustic vortices is in high-speed communications and transmission applications, as the orbital angular moment of the vortex beams can serve as an information carrier.[16–20] Shi *et al.* showcased an advanced approach to communication by employing the orbital angular momentum produced by acoustic vortex beams with a one-order enhancement of the data transmission rate.[21] Furthermore, in another study, an orbital angular momentum prism of an acoustic vortex beam was used to accurately and quantitatively detect vortex patterns in an efficient manner. The system transforms the swirling vortices into plane waves that pass through at varying angles of refraction. This process facilitates the quick and efficient interpretation of the data encoded within each vortex.[22] In addition, various research initiatives have investigated the application of acoustic vortices in the biomedical sector.[23–25] For instance, some studies utilized a synergistic tumor therapy approach by combining high-intensity focused ultrasound with a singular acoustic vortex beam emitted by a 16-element spherical concave ultrasound transducer at 660 kHz, which proved to effectively reduce clot debris and enhance thrombolytic efficacy.[26] In a separate effort, Wu *et al.* engineered a focused acoustic vortex system dedicated to enhanced cancer treatment, creating an ultrasound field with a hollow cylindrical focal area. The system, employing a 16-element array transducer at 500 Hz in tandem with phase change nanodroplets, inflicted greater damage on tumor tissue when compared with standard focused ultrasound at identical acoustic pressures.[27] Similarly, Jiménez-Gambín *et al.* leveraged a phase-reversed acoustic hologram in conjunction with a singular beam acoustic vortex. This combination was aimed at correcting aberrations introduced by the human skull, thereby facilitating targeted ultrasound wave focusing within the skull's cranial cavity. The creation of this acoustic vortex was achieved using a spherically focused piezoelectric transducer functioning at 500 kHz.[28]

Although considerable research has focused on acoustic vortices, the majority of studies have employed them at low intensities.[29,30] The generation of acoustic vortices at higher intensities could be more advantageous for biomedical ultrasound-related applications. For example, a higher acoustic energy can facilitate the production of cavitation, an effect beneficial for many ultrasonic medical applications, including tumor ablation[31,32] and tissue liquefaction.[33–35] In addition, the vast majority of the existing devices are limited to the use of a single vortex beam, which often results in limited efficiency or capacity. There are several challenges associated with the incorporation of multiple vortices in a simple device to broaden its functionality. These include the necessity for complicated transducer arrays[36–38] and potential operational limitations dictated by factors such as particle size and the propagation medium. These factors can lead to acoustic wave reflection and refraction, resulting in the distortion of the acoustic beam shape,[39,40] and the introduction of a focusing mechanism further complicates their operation. Hence, increasing the number of vortices produced by a single acoustic lens has the potential to broaden the functionality and adaptability of the existing available devices in various fields.

In this paper, we demonstrate the successful generation of an underwater regular and focused acoustic double vortex using a customized vortex lens based on a single lens fabricated with a stereolithography (SLA) printer. The lens design was based on the pressure field multiplexing concept, where the lens integrates the pressure fields from separate vortices to achieve a combined output capable of emitting intertwined pressure fields. The efficacy of the lens was evaluated through both computational simulations using finite element analysis and experimental tests involving hydrophone measurements. The results indicate that the acoustic double vortex lens design is proficient in producing acoustical double vortices in both standard and concentrated manners. The technique offers an efficient and straightforward solution for the creation of acoustic double vortices. Such a method holds promise for numerous practical applications, including communication technologies, biomedical fields, and the manipulation and rotational control of particles.

II. NUMERICAL ANALYSIS

A. Acoustic lens design

To generate an acoustic vortex, an acoustic lens with a spiral phase profile needs to be designed, which imposes an azimuthally varying thickness. The thickness variation of the lens imparts a certain phase delay when acoustic waves travel across the lens, thereby forming certain pressure fields at the far field. For a single vortex lens, the shape follows a simple azimuthal changing profile [Fig. 1(a)]. To incorporate a double vortex from a single underlying lens, the acoustic fields of two vortex beams with different centers are first multiplexed to create a combined acoustic pressure field, as shown in Fig. 1(b). The thickness at different locations of the lens can then be obtained by relating the phase map of each single vortex beam $\phi_{1,2}(x, y)$ as follows:[41,42]

$$h = h_{max}[\sin(\phi_1(x, y)) + \sin(\phi_2(x, y))], \quad (1)$$

$$\phi_{1,2}(x, y) = \frac{arc\,tan\,2(x + m_{1,2}, y) + \pi}{2}, \phi_{1,2}(x, y) \in [0, 2\pi], \quad (2)$$

where h_{max} is the maximum thickness of the lens that corresponds to a 2π phase delay and $m_{1,2}$ is the phase singularity offset for each vortex beam. Equations (1) and (2) allow for the generation of the required spiral phase profile varying from 0 to 2π. A frequency domain simulation was performed in COMSOL using a parametric sweep to ascertain the requisite thickness needed to achieve a total phase change of 2π. An initial height, h_0, of 4 mm as a uniform lens base was selected to simplify the 3D printing process. The initial setting of the base height led to setting the maximum height to $h_{max} = 8.1$ mm. A customized code that incorporates the design equations and scripts for transforming surfaces into three-dimensional solids has been utilized to produce the acoustic vortex lens design. The design was then exported as STL files, formatted for 3D printing, as shown in Fig. 1(c).

In the case of the focused versions of the acoustic vortex, a similar design approach was used. The pressure field multiplexing was performed by creating a pressure distribution related to acoustic vortex generation combined with another one that presents a pressure focal profile. Due to the linearity of the acoustic waves, the total field will be a multiplexed pressure field that exhibits both features
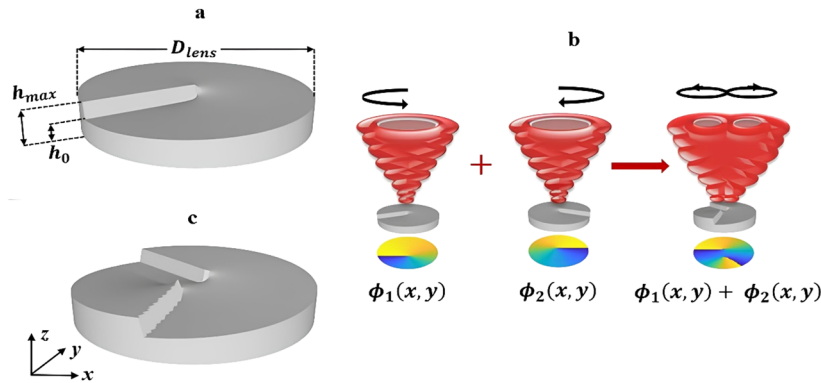
FIG. 1. Designed acoustic vortex lens and the concept behind it. (a) The geometry of a simple beam vortex lens. (b) The formation of double acoustic vortex by field multiplexing. (c) The geometry of a double beam vortex lens.

simultaneously. The following concave shape equation was included to take into consideration the focal length and the location of the overall lens:

$$\frac{f_l}{c_m} = \frac{\sqrt{R_{pr}^2 + (f_l - R_{cr} + \sqrt{R_{Cr}^2 - R_{pr}^2})^2}}{c_m} + \frac{R_{cr} - \sqrt{R_{cr}^2 - R_{pr}^2}}{c_l}, \quad (3)$$

where R_{pr} is the radius of the aperture, f_l is the focal length of the lens, R_{cr} is the radius of the curvature of the lens, while c_m and c_l are the speed of sound of the surrounding material and lens, respectively. It is worth noting that the first-order Taylor series approximation of the square root function, as presented in Eq. (3), results in the widely recognized form for R_{cr} of an acoustic lens used in various studies $R_{cr} = f_l \left(1 - \frac{c_m}{c_l}\right)$.[43,44]

B. Numerical simulation

The performance of the proposed lens in generating a double beam acoustic vortex was assessed using finite element simulations in COMSOL Multiphysics v6.1. Using the same software, the STL file of the 3D generated lens was imported and a linear isotropic elastic material property was assigned to it. In the simulation, a total diameter of D_{lens} = 49 mm was utilized for the lens. It was entirely encompassed by a cylindrical space measuring 100 mm in height (H) and 49 mm in diameter, which was concentric with the lens. A linear elastic model for the fluid was used in the simulation. Owing to the small attenuation in the lens material and the background medium, loss is not considered in the numerical model. A free adaptive tetrahedral element mesh was implemented, with the largest element sizing up to 0.5 mm, paired with a curvature factor of 0.3. The density and speed of sound assigned to the imported lens and the surrounding medium correspond to the cured SLA resin and water properties, which are ρ_l = 1178 kg/m^3, c_l = 2591 m/s and ρ_m = 1000 kg/m^3, c_m = 1490 m/s, respectively, to accurately represent the model.[45] The pressure acoustics–frequency domain was used for calculating the pressure distribution and phase variations produced by the lens. The equation that formed the basis of the numerical

analysis uses the inhomogeneous Helmholtz equation. For a lossless adiabatic flow, it reads

$$\Delta \cdot \left(-\frac{1}{\rho} \Delta p_t\right) - \frac{k_{eq}^2 p_t}{\rho} = 0, \quad (4)$$

where the material density is donated by ρ, the total pressure is presented by p_t, while k_{eq} represents the wave number that contains both the ordinary wave number $k = \frac{\omega}{c_l}$ and the out-of-plane wave number k_z, where ω is the angular frequency and c_l is the lens speed of sound. To study the wave field generated by the lens, a plane wave radiation boundary condition with an acoustic excitation frequency of 1 MHz was established at the lens's base. Impedance boundary conditions were placed along the cylindrical area's perimeter and apex to eliminate unwanted reflections during the simulation, while a sound hard boundary condition was selected for its bottom maintaining a realistic representation of actual conditions. Simulations were conducted on four different versions of acoustic vortex lenses: a single vortex, a double vortex, and a focused single and double vortex with a curvature radius of R_{cr} = 28 mm, respectively.

As shown in Fig. 2, the simulation results in the x–y plane away from the lens across these scenarios revealed that the variations in phase and amplitude were consistent with anticipated outcomes drawn from both theoretical insights and the existing literature on single acoustic beam vortices[46–48] and double optical vortices,[49] as well as from acoustic-related theoretical predictions. In addition, the single vortex's pressure field demonstrated a gradual phase shift from 0 to 2π, including the anticipated singularity at its core. Similarly, this pressure profile featured a pronounced pressure ring, formed due to the differential pressure and angular momentum of the vortex, amid a zone of zero pressure at the center. The double vortex replicated these patterns, with the phase shifting twice smoothly between 0 and 2π and singularities at the center of each vortex. The pressure profiles of the double vortex confirmed the expected outcomes as well, with prominent pressure rings from each vortex merging to create a figure-of-eight pattern, while the centers maintained zero pressure.
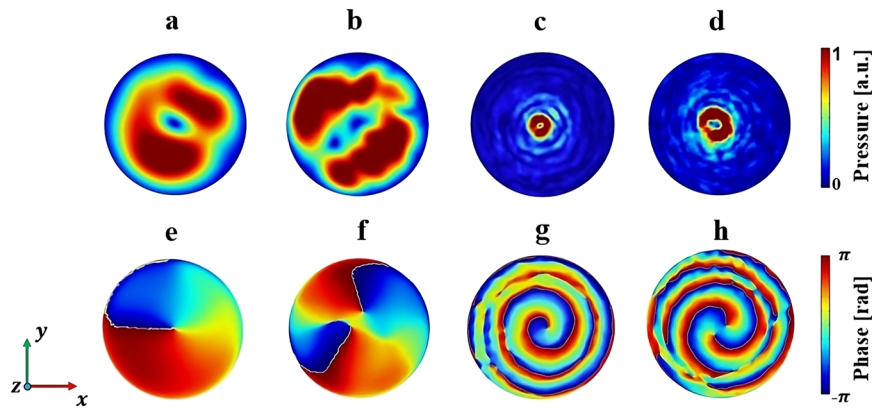
FIG. 2. Simulated results of (a)–(d) normalized pressure and (e)–(h) phase profile in the x–y plane at z = 65 mm of single vortex, double vortex, focused single vortex, and focused double vortex, respectively.
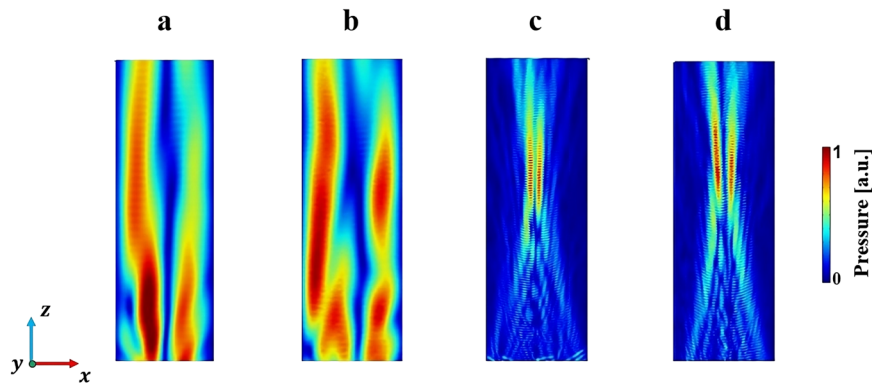

FIG. 3. Simulated results of normalized pressure in the x–z plane of (a) single vortex, (b) double vortex, (c) focused single vortex, and (d) focused double vortex.

To better visualize the performance of the lenses, the pressure fields in the x–z plane at y = 0 mm across these scenarios are presented in Fig. 3 as the waves propagate from the lens to the far field. The presented area spans 49 mm along the x-axis and 100 mm along the y-axis. In the case of single and double vortices, a high pressure region generated due to the angular momentum of the vortices can be observed along the plane with a pressure minimum situated at the center of it. For the case of focalized lenses, the majority of the acoustic pressure is generated at the design focal point of the lenses as expected with a slight variation due to the nature of the vortex. Compared to the normal vortex lenses, it can be seen that the focused lenses are capable of effectively focalizing energy at the pre-designed
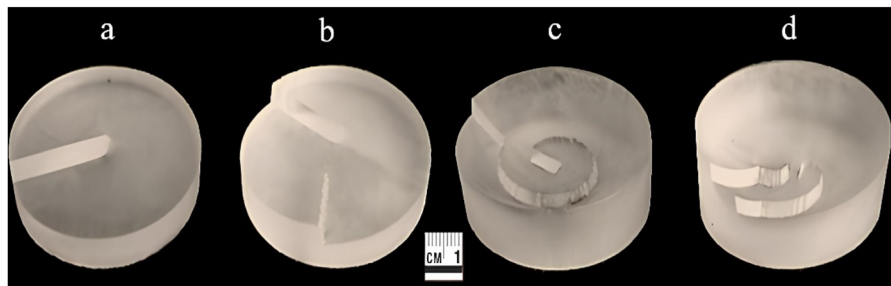

FIG. 4. Completed 3D-printed lenses. (a) Single vortex, (b) double vortex, (c) focused single vortex, and (d) focused double vortex.
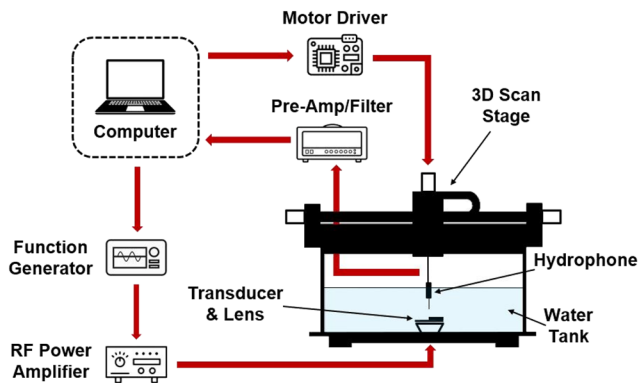
03 April 2024 13:59:17

FIG. 5. Schematic of the measurement setup used for the vortex data collection.

focal point of the lens, thus providing a convenient way of tailoring the focusing effect based on the desired application.

III. EXPERIMENTAL RESULTS

To evaluate the performance of the different acoustic vortex lens configurations, a prototype was produced for each design using a Formlabs stereolithography 3D printer, which offers a high print resolution of up to 25 μm. Such a resolution is well below the corresponding wavelength of the acoustic waves, thereby ensuring the smoothness of the fabricated lenses and helping to minimize undesired diffractions. All lenses had a consistent diameter of 49 mm to match the transducer's size. The variation designed for focusing had a curvature radius of 28 mm. The lenses had a base height of 4 mm and a peak height of 8.1 mm. Figure 4 illustrates the completed 3D-printed lenses designed for both single and double vortices.

Following their printing, the lenses were mounted on a ceramic circular piezoelectric transducer (SMR, Davenport, FL). This transducer has a diameter of 49 mm and a thickness of 2 mm, with a 1 MHz resonance frequency to provide the necessary acoustic actuation. A function generator (RIGOL DG4162, Portland, OR) was

used to generate a sinusoidal burst signal with a 20% duty cycle and shaped by a Gaussian envelope. The output signal was then amplified through an RF power amplifier (ENI 3200L, Renton, WA) to ensure sufficient acoustic wave intensity at the bottom of the lens.

The generated acoustic field during each experiment was measured using a hydrophone (Acoustics NH0500, Dorchester, UK) mounted on a 3D scan stage. The schematic of the measurement setup is shown in Fig. 5. The generated sinusoidal burst input wave was used to differentiate the direct-transmitted signal emitted from the lens from the reflected ones generated by the boundaries since these signals have some time delay. The hydrophone was used for the collection of the initial experimental data through a 5 mm needle hydrophone, which was then processed using appropriate software. To preserve the integrity of the measured signal and to isolate it from unwanted background noise and secondary reflections, a combination of a 10 Hz high-pass Butterworth filter and a custom-made MATLAB script was utilized. The script was used to keep the main signal originating from the lens intact by using a sliding window technique, which effectively discarded any data points not associated with the primary event, such as the secondary reflections generated from the water tank walls. The implementation of the filtering step was essential to achieve a precise phase. The data of this phase were then derived by employing the signal from the function generator as a reference point.

During the experimental process, a thorough scan consisting of an 80-by-80 step matrix in both x and y directions was performed with 125 000 data points recorded and extracted through the use of oscilloscope memory at each position on the hydrophone's scanning trajectory. The configured scanning array comprehensively encompassed the vortex lens and its surrounding field, facilitating an enhanced analysis and visual representation of both amplitude and phase information generated by the lens. The obtained experimental results for the different lens configurations for both phase and pressure amplitude variations at z = 65 mm, which corresponds to the focal depth of the focal lenses, are shown in Fig. 6.

Experimental outcomes for all lens configurations demonstrated good agreement with theoretical and simulation results. In the case of a single vortex, the phase variation was observed to range between 0 and 2π concentrically around the core, and the pressure
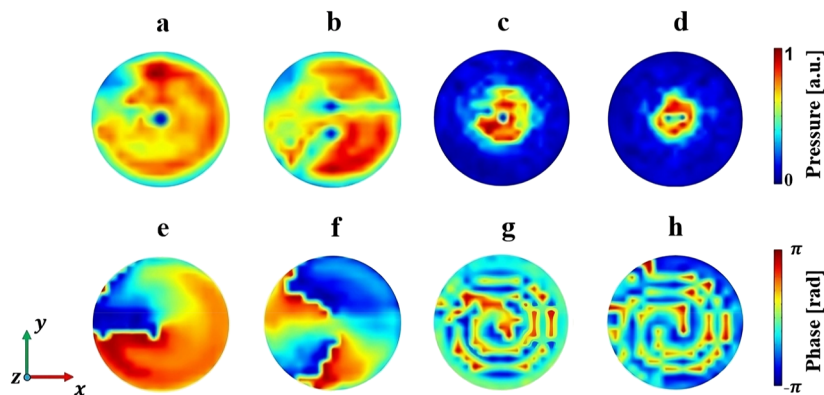

FIG. 6. Experimental results of (a)–(d) the normalized pressure and (e)–(h) the phase profile in the x–y plane at z = 65 mm of single vortex, double vortex, focused single vortex, and focused double vortex, respectively.

profile exhibited a point of zero pressure at the lens's center. With regard to the double vortex configuration, the phase pattern resembled that of the single vortex, yet it was replicated at the center of each of the two vortices. This duplicating effect was similarly reflected in the pressure profile for the double vortex, where a zero-pressure point can be clearly seen at the central point of each vortex. The experimental findings indicate that by meticulously designing and integrating different acoustic structures, it is feasible to create intricate sound patterns, such as the case with the double vortex, while still maintaining a straightforward design and fabrication process.

Nonetheless, some inconsistencies were observed when comparing theoretical predictions with experimental outcomes. Specifically, the phase spirals produced were not as refined, exhibiting insufficient smoothness and an indistinct central phase singularity in contrast to the simulations. In experiments with the focused acoustic vortex lens, the actual focal lengths did not exactly match the one seen in the simulation, and there was a minor misalignment of the produced vortex beam from the center of the lens, especially for the double vortex case. The discrepancies observed between our simulated results and the experimental measurements could have several underlying causes. One potential source of error may be the slight variation between the actual properties of the cured resin compared to the reported data. In addition, the limited scanning resolution of the hydrophone could lead to some inconsistencies in the measured fields. Other reasons for the inconsistency can also be attributed to the fluctuation generated by the transducer throughout the experimental procedures and the minor deviations in the phase profile due to imperfections during the printing process. Nevertheless, the aforementioned experimental errors could be reduced by improving the efficiency of the transducer, lens fabrication, and scanning system and reducing step size during collecting the data even though it could be computationally taxing.

IV. CONCLUSION

In this research, an acoustic lens capable of creating a double vortex was both theoretically conceived and experimentally verified. The proposed lens design incorporated a concave element into the initial model, resulting in a version capable of concentrating double acoustic vortices. This method holds promise for greater practicality and effectiveness as it dispenses with the complicated arrays of transducers or intricate experimental setups previously required to generate such complicated vortex patterns, applicable to both single and twin vortex configurations. Custom scripts were employed for theoretical modeling, while the COMSOL software facilitated pressure acoustics–frequency domain simulations to study the different variations of the proposed acoustic lens. These simulations confirmed that the performance of the proposed lens design and its variations aligned with the predictions based on theoretical understanding and the body of knowledge surrounding both single acoustic and double optical vortices. Employing a PZT transducer with a resonance frequency of 1 MHz, the results confirmed the formation of a double-vortex profile. This was evidenced by distinct circular pressure patterns with a phase spiral variation from 0 to 2π at the core of each vortex. The findings were further supported by an experimental validation approach using 3D printing

and hydrophone measurement. Our research broadens the functionality beyond traditional single-beam acoustic vortices, enhancing their significance in the realms of biomedicine, communications, and the active control of *in vivo* entities by introducing more vortices and enabling the control of their intensities.[50–52]

The outcomes and demonstrations of this study shed new light on the ultrasonic domain and pave the way for potential interesting work related to acoustic vortex and its use in 3D fields through double acoustic vortex generation. The suggested method offers advantages across a broad spectrum of uses. For instance, a single, prefabricated lens could simplify complex scenarios involving a double vortex, which would greatly simplify the need for intricate tweezer systems and enhance both the efficiency and simplicity of the experimental setup. Furthermore, the proposed lens design allows the tuning of the focal distance in the case of the focusing version so that the acoustic energy can be concentrated at a desired location. Such flexibility could be very helpful in acoustofluidics, where this lens could enable selective manipulation of particles of different sizes and characteristics due to its ability to focus energy more intensely at a specific location.[53] In addition, the vortex's angular momentum could be harnessed to dislodge blood clots in human arteries.[54] Moreover, while a topological charge of one is demonstrated in the current work, extending the design for other vortex beams with different topological charges is straightforward. The lens design proposed in this paper can also be extended to incorporate more than two vortices, which will broaden the bandwidth and capacity of vortex-based particle manipulation and acoustic communications. In principle, the proposed approach can be integrated with iterative algorithms or inverse design techniques for multiplexed vortex generations at different frequencies, as has been demonstrated in acoustic holograms.[55–57] It is hoped that the proposed approach provides a versatile means of synthesizing acoustic vortex beams with distinct features and will benefit a range of applications as well as the future enhancement of medical instruments.

AUTHOR DECLARATIONS

Conflict of Interest

The authors have no conflicts to disclose.

Author Contributions

Chadi Ellouzi: Data curation (equal); Formal analysis (equal); Writing – original draft (equal); Writing – review & editing (equal). **Ali Zabihi**: Data curation (equal); Formal analysis (equal); Writing – review & editing (equal). **Farhood Aghdasi**: Data curation (equal); Formal analysis (equal); Writing – review & editing (equal).

03 April 2024 13:59:17

DATA AVAILABILITY

The data that support the findings of this study are available from the corresponding authors upon reasonable request.

REFERENCES

[1] X.-D. Fan, Z. Zou, and L. Zhang, "Acoustic vortices in inhomogeneous media," Phys. Rev. Res. **1**(3), 032014 (2019).

[2] Y. Fu, C. Shen, X. Zhu, J. Li, Y. Liu, S. A. Cummer, and Y. Xu, "Sound vortex diffraction via topological charge in phase gradient metagratings," Sci. Adv. **6**(40), eaba9876 (2020).

[3] C. Zhou, Q. Wang, S. Pu, Y. Li, G. Guo, H. Chu, Q. Ma, J. Tu, and D. Zhang, "Focused acoustic vortex generated by a circular array of planar sector transducers using an acoustic lens, and its application in object manipulation," J. Appl. Phys. **128**(8), 084901 (2020).

[4] M. Cromb, G. M. Gibson, E. Toninelli, M. J. Padgett, E. M. Wright, and D. Faccio, "Amplification of waves from a rotating body," Nat. Phys. **16**(10), 1069–1073 (2020).

[5] C. Liu, Y. Ye, and J. H. Wu, "Tunable broadband acoustic vortex generator with multiple orders based on Mie resonances structure," Adv. Mater. Technol. **8**(13), 2202082 (2023).

[6] I. Martynyuk-Lototska, M. Kostyrko, D. Adamenko, I. Skab, and R. Vlokh, "Generation of acoustic vortices and acousto-optic interactions with acoustic vortex beams," Appl. Opt. **62**(14), 3643 (2023).

[7] J.-L. Thomas and R. Marchiano, "Pseudo angular momentum and topological charge conservation for nonlinear acoustical vortices," Phys. Rev. Lett. **91**(24), 244302 (2003).

[8] J. Zhang, K. Yang, H. Luo, P. Li, F. Wen, Y. Gu, and Z. Wu, "Modulation of orbital angular momentum of vortex beam based on ordered pinhole screens," Results Phys. **51**, 106713 (2023).

[9] Y. Li, G. Guo, J. Tu, Q. Ma, X. Guo, D. Zhang, and O. A. Sapozhnikov, "Acoustic radiation torque of an acoustic-vortex spanner exerted on axisymmetric objects," Appl. Phys. Lett. **112**(25), 254101 (2018).

[10] C. R. P. Courtney, C. E. M. Demore, H. Wu, A. Grinenko, P. D. Wilcox, S. Cochran, and B. W. Drinkwater, "Independent trapping and manipulation of microparticles using dexterous acoustic tweezers," Appl. Phys. Lett. **104**(15), 154103 (2014).

[11] Z. Y. Hong, J. F. Yin, W. Zhai, N. Yan, W. L. Wang, J. Zhang, and B. W. Drinkwater, "Dynamics of levitated objects in acoustic vortex fields," Sci. Rep. **7**(1), 7093 (2017).

[12] Y. Gu, C. Chen, J. Rufo, C. Shen, Z. Wang, P.-H. Huang, H. Fu, P. Zhang, S. A. Cummer, Z. Tian, and T. J. Huang, "Acoustofluidic holography for micro- to nanoscale particle manipulation," ACS Nano **14**(11), 14635–14645 (2020).

[13] J. Li, A. Crivoi, X. Peng, L. Shen, Y. Pu, Z. Fan, and S. A. Cummer, "Three dimensional acoustic tweezers with vortex streaming," Commun Phys **4**(1), 113 (2021).

[14] M. Baudoin, J.-L. Thomas, R. A. Sahely, J.-C. Gerbedoen, Z. Gong, A. Sivery, O. B. Matar, N. Smagin, P. Favreau, and A. Vlandas, "Spatially selective manipulation of cells with single-beam acoustical tweezers," Nat. Commun. **11**(1), 4244 (2020).

[15] W.-C. Lo, C.-H. Fan, Y.-J. Ho, C.-W. Lin, and C.-K. Yeh, "Tornado-inspired acoustic vortex tweezer for trapping and manipulating microbubbles," Proc. Natl. Acad. Sci. U. S. A. **118**(4), e2023188118 (2021).

[16] G. Guo, X. Li, Q. Wang, Y. Li, H. Chu, Q. Ma, J. Tu, and D. Zhang, "Spectrum decomposition-based orbital angular momentum communication of acoustic vortex beams using single-ring transceiver arrays," IEEE Trans. Ultrason. Ferroelectrics Freq. Control **68**(4), 1399–1407 (2021).

[17] Z.-Y. Guo, H.-J. Liu, J.-J. Li, H.-P. Zhou, K. Guo, and J. Gao, "Research progress of applications of acoustic-vortex information," Acta Phys. Sin. **69**(24), 244301 (2020).

[18] S. Guo, Z. Ya, P. Wu, and M. Wan, "A review on acoustic vortices: Generation, characterization, applications and perspectives," J. Appl. Phys. **132**(21), 210701 (2022).

[19] X. Jiang, B. Liang, J. Cheng, and C. Qiu, "Twisted acoustics: Metasurface-enabled multiplexing and demultiplexing," Adv. Mater. **30**(18), 1800257 (2018).

[20] C. Zhang, X. Jiang, J. He, Y. Li, and D. Ta, "Spatiotemporal acoustic communication by a single sensor via rotational Doppler effect," Adv. Sci. **10**(10), 2206619 (2023).

[21] C. Shi, M. Dubois, Y. Wang, and X. Zhang, "High-speed acoustic communication by multiplexing orbital angular momentum," Proc. Natl. Acad. Sci. U. S. A. **114**(28), 7250–7253 (2017).

[22] X. Jiang, N. Wang, C. Zhang, X. Fang, S. Li, X. Sun, Y. Li, D. Ta, and W. Wang, "Acoustic orbital angular momentum prism for efficient vortex perception," Appl. Phys. Lett. **118**(7), 071901 (2021).

[23] M. A. Ghanem, A. D. Maxwell, Y.-N. Wang, B. W. Cunitz, V. A. Khokhlova, O. A. Sapozhnikov, and M. R. Bailey, "Noninvasive acoustic manipulation of objects in a living body," Proc. Natl. Acad. Sci. U. S. A. **117**(29), 16848–16855 (2020).

[24] A. Riaud, M. Baudoin, O. Bou Matar, L. Becerra, and J.-L. Thomas, "Selective manipulation of microscopic particles with precursor swirling Rayleigh waves," Phys. Rev. Appl. **7**(2), 024007 (2017).

[25] D. Baresch and V. Garbin, "Acoustic trapping of microbubbles in complex environments and controlled payload release," Proc. Natl. Acad. Sci. U. S. A. **117**(27), 15490–15496 (2020).

[26] S. Guo, X. Wang, X. Guo, Z. Ya, P. Wu, A. Bouakaz, and M. Wan, "Decreased clot debris size and increased efficiency of acoustic vortex assisted high intensity focused ultrasound thrombolysis," J. Appl. Phys. **128**(9), 094901 (2020).

[27] P. Wu, Z. Ya, Y. Li, M. Zhu, L. Zhang, Y. Zong, S. Guo, and M. Wan, "Focused acoustic vortex-regulated composite nanodroplets combined with checkpoint blockade for high-performance tumor synergistic therapy," ACS Appl. Mater. Interfaces **14**(27), 30466–30479 (2022).

[28] S. Jiménez-Gambín, N. Jiménez, and F. Camarena, "Transcranial focusing of ultrasonic vortices by acoustic holograms," Phys. Rev. Appl. **14**(5), 054070 (2020).

[29] C. Wilson and M. J. Padgett, "A polyphonic acoustic vortex and its complementary chords," New J. Phys. **12**(2), 023018 (2010).

[30] B. Zhang, H. Wu, H. Kim, P. J. Welch, A. Cornett, G. Stocker, R. G. Nogueira, J. Kim, G. Owens, P. A. Dayton, Z. Xu, C. Shi, and X. Jiang, "A model of high-speed endovascular sonothrombolysis with vortex ultrasound-induced shear stress to treat cerebral venous sinus thrombosis," Research **6**, 0048 (2023).

[31] K. F. Chu and D. E. Dupuy, "Thermal ablation of tumours: Biological mechanisms and advances in therapy," Nat. Rev. Cancer **14**(3), 199–208 (2014).

[32] M. Nikfarjam, V. Muralidharan, and C. Christophi, "Mechanisms of focal heat destruction of liver tumors," J. Surg. Res. **127**(2), 208–223 (2005).

[33] T. D. Khokhlova, Y.-N. Wang, J. C. Simon, B. W. Cunitz, F. Starr, M. Paun, L. A. Crum, M. R. Bailey, and V. A. Khokhlova, "Ultrasound-guided tissue fractionation by high intensity focused ultrasound in an in vivo porcine liver model," Proc. Natl. Acad. Sci. U. S. A. **111**(22), 8161–8166 (2014).

[34] S. A. Curley, J. C. Cusack, K. K. Tanabe, and L. M. Ellis, "Advances in the treatment of liver tumors," Curr. Probl. Surg. **39**(5), 461–571 (2002).

[35] T. J. Vogl, R. Straub, K. Eichler, O. Söllner, and M. G. Mack, "Colorectal carcinoma metastases in liver: Laser-induced interstitial thermotherapy—Local tumor control rate and survival data," Radiology **230**(2), 450–458 (2004).

[36] J. F. Pazos-Ospina, F. Quiceno, J. L. Ealo, H. R. D. Muelas, and J. Camacho, "Focalization of acoustic vortices using phased array systems," Phys. Procedia **70**, 183–186 (2015).

[37] J. F. Pazos-Ospina, J. L. Ealo, and E. E. Franco, "Characterization of phased array-steered acoustic vortex beams," J. Acoust. Soc. Am. **142**(1), 61–71 (2017).

[38] M. E. Kelly and C. Shi, "Design and simulation of acoustic vortex wave arrays for long-range underwater communication," JASA Express Lett. **3**(7), 076001 (2023).

[39]S. Pu, G. Guo, X. Guo, C. Zhou, Y. Li, Q. Ma, J. Tu, and D. Zhang, "Auto-focusing acoustic-vortex tweezers for obstacle-circumventing manipulation," J. Appl. Phys. **130**(23), 234903 (2021).

[40]S. Jiménez-Gambín, N. Jiménez, J. M. Benlloch, and F. Camarena, "Holograms to focus arbitrary ultrasonic fields through the skull," Phys. Rev. Appl. **12**(1), 014016 (2019).

[41]E. Agiasofitou and M. Lazar, "Mathematical modeling of electro-elastic dislocations in piezoelectric materials," PAMM **22**(1), e202200167 (2023).

[42]T. Kusaka and T. Tanaka, "Fast and accurate approximation methods for trigonometric and arctangent calculations for low-performance computers," Electronics **11**(15), 2285 (2022).

[43]J. Jang and J. Chang, "Design and fabrication of double-focused ultrasound transducers to achieve tight focusing," Sensors **16**(8), 1248 (2016).

[44]Y. Hosono, Y. Yamashita, and K. Itsumi, "Effects of fine metal oxide particle dopant on the acoustic properties of silicone rubber lens for medical array probe," IEEE Trans. Ultrason. Eng. **54**(8), 1589–1595 (2007).

[45]M. Bakaric, P. Miloro, A. Javaherian, B. T. Cox, B. E. Treeby, and M. D. Brown, "Measurement of the ultrasound attenuation and dispersion in 3D-printed photopolymer materials from 1 to 3.5 MHz," J. Acoust. Soc. Am. **150**(4), 2798–2805 (2021).

[46]H. Tang, Z. Chen, N. Tang, S. Li, Y. Shen, Y. Peng, X. Zhu, and J. Zang, "Hollow-out patterning ultrathin acoustic Metasurfaces for multifunctionalities using soft fiber/rigid bead networks," Adv. Funct. Mater. **28**(36), 1801127 (2018).

[47]Z. Zou, R. Lirette, and L. Zhang, "Orbital angular momentum reversal and asymmetry in acoustic vortex beam reflection," Phys. Rev. Lett. **125**(7), 074301 (2020).

[48]C. Liu, H. Long, C. Ma, Y. Jia, C. Shao, Y. Cheng, and X. Liu, "Broadband acoustic vortex beam generator based on coupled resonances," Appl. Phys. Lett. **118**(14), 143503 (2021).

[49]M. Guo, W. Le, C. Wang, G. Rui, Z. Zhu, J. He, and B. Gu, "Generation, topological charge, and orbital angular momentum of off-axis double vortex beams," Photonics **10**(4), 368 (2023).

[50]A. Marzo, M. Caleap, and B. W. Drinkwater, "Acoustic virtual vortices with tunable orbital angular momentum for trapping of Mie particles," Phys. Rev. Lett. **120**(4), 044301 (2018).

[51]S. Gao, Y. Li, C. Ma, Y. Cheng, and X. Liu, "Emitting long-distance spiral airborne sound using low-profile planar acoustic antenna," Nat. Commun. **12**(1), 2006 (2021).

[52]R. Zhang, H. Guo, W. Deng, X. Huang, F. Li, J. Lu, and Z. Liu, "Acoustic tweezers and motor for living cells," Appl. Phys. Lett. **116**(12), 123503 (2020).

[53]D. J. Collins, B. L. Khoo, Z. Ma, A. Winkler, R. Weser, H. Schmidt, J. Han, and Y. Ai, "Selective particle and cell capture in a continuous flow using micro-vortex acoustic streaming," Lab Chip **17**(10), 1769–1777 (2017).

[54]S. Guo, Z. Ya, P. Wu, L. Zhang, and M. Wan, "Enhanced sonothrombolysis induced by high-intensity focused acoustic vortex," Ultrasound Med. Biol. **48**(9), 1907–1917 (2022).

[55]I. Meighan, E. De Asis, and C. Shen, "Multiplexed acoustic holography using an iterative angular spectrum approach," The J. Acoust. Soc. Am. **150**(4_Supplement), A147 (2021).

[56]Y. Zhu, N. J. Gerard, X. Xia, G. C. Stevenson, L. Cao, S. Fan, C. M. Spadaccini, Y. Jing, and B. Assouar, "Systematic design and experimental demonstration of transmission-type multiplexed acoustic metaholograms," Adv. Funct. Mater. **31**(27), 2101947 (2021).

[57]Q. Lin, R. Zhang, F. Cai, Y. Chen, J. Ye, J. Wang, H. Zheng, and H. Zhang, "Multi-frequency acoustic hologram generation with a physics-enhanced deep neural network," Ultrasonics **132**, 106970 (2023).